Influence of Crystallization on Intercalation, Morphology, and Mechanical Properties of Polypropylene/Clay Nanocomposites

Pralay Maiti, Pham Hoai Nam, and Masami Okamoto*

Advanced Polymeric Materials Engineering, Graduate School of Engineering, Toyota Technological Institute, Hisakata 2-12-1, Tempaku, Nagoya 468-8511, Japan

Naoki Hasegawa and Arimitsu Usuki

Toyota Central R&D Labs., Inc., Nagakute, Aichi 480-1192, Japan

Received May 15, 2001; Revised Manuscript Received December 27, 2001

ABSTRACT: Intercalated nanocomposites of polypropylene (PP)/clay (PPCNs) were prepared by a melt extrusion process using maleic anhydride modified PP (PP-MA) and organophilic clay. The extent of intercalation of PP-MA chains in the space between silicate galleries increased with crystallization temperature T_c and decreased as clay content increased. As compared to matrix PP-MA, the dispersed clay particles in the PP-MA matrix acted as a nucleating agent and lowered the spherulite dimension with increasing clay content as revealed by light scattering experiments and polarizing optical microscopy. The PPCN crystallized at high T_c showed that a certain extent of segregation of the dispersed clay particles takes place around the boundary of the spherulites (interspherulite). Extensive intercalation occurred during crystallization, especially at high T_c due to the long time for full solidification of the melt. The degree of intercalation of PP-MA chains in the silicate galleries strongly depends on the time in the molten state. The effect of the intercalation through organophilic interaction on the dynamic storage modulus of the PPCNs crystallized in the temperature range of 70−130 °C has been emphasized.

Introduction

Intercalation of polymer melts in layered silicates of synthetically modified clay such as lipophilized montmorillonite has recently become better understandable as a good tool to prepare composite material exhibiting excellent thermal, gas barrier, and mechanical properties.[1,2]

In our previous paper, we have prepared successfully intercalated nanocomposites of polypropylene (PP)/clay (PPCNs) using maleic anhydride modified PP (PP-MA) and organophilic clay.[3−5] From transmission electron microscopy (TEM) observation, the silicate layers of about 150 nm length and about 4 nm thickness are finely dispersed in the PP-MA matrix. In the intercalated PPCNs, the correlation length of the dispersed clay particles of 30−50 nm was comparable to the radius of gyration of the polymer, and one or several extended PP-MA chains were inserted between the silicate galleries.[5]

Then, we demonstrated the hierarchical structure of the intercalated PPCNs viewed on scale from the structure of confined PP-MA chains in the space of the silicate galleries (intercalating sites) of 2−3 nm width to crystalline lamellae of 7−15 nm thickness and spherulitic texture of 10 μm diameter.[5] However, a detailed understanding of the effect on crystallization of the nanoscale confinement of polymer molecules and subsequent structure, morphology, and mechanical properties is not yet well understood. To control the fine structure and thereby the mechanical properties, we should clarify the effect of the dispersed clay particles of nanometer dimension and the intercalation of PP-MA chains into silicate galleries on the crystallization of PPCNs.

* Corresponding author: Tel +81-52-809-1861; fax +81-52-809-1864; e-mail okamoto@toyota-ti.ac.jp.

In this paper, first we present the fine structure, morphology, and kinetics of crystallization of the intercalated PPCNs having different clay content. Second, how does the crystallization control the fine structure and morphology of the PPCNs and the effect of clay content on the intercalation? A plausible mechanism of intercalation through crystallization has been proposed. Finally, the effect of intercalation on the mechanical and thermal properties of PPCN has been discussed.

Experimental Section

Materials and Crystallization. The PPCNs used in this study were same materials in our previous studies.[4,5] Maleic anhydride grafted polypropylene (PP-MA) from Exxon Chemical was used as the matrix ($M_w = 1.95 \times 10^5$, $M_w/M_n = 2.98$, and MA content = 0.2 wt %). The PPCNs were prepared through the melt extrusion method with PP-MA and three different clay (montmorillonite intercalated with stearylammonium ion) contents of 2, 4, and 7.5 wt % and henceforth will be termed as PPCN2, PPCN4, and PPCN7.5, respectively, using a twin screw extruder (TEX30α-45.5BW, Japan Steel Works Ltd.) operating at 200 °C. The extruded and pelletized strands were dried under vacuum at 80.0 °C to remove residual water. The sample of $10 \times 10 \times 0.5$ mm^3 size was cut from a compression-molded sheet and melted at 190 °C on a hot plate for 5 min (to remove the thermal history) and quickly transferred to a thermostated hot stage (Linkam LK600PM, Linkam Scientific Instruments, Ltd.) set at the predetermined temperature and crystallized until full solidification (confirmed from the kinetics of crystallization using a polarizing optical microscope (POM)). The crystallized samples were characterized using wide-angle X-ray diffraction (WAXD), TEM observation, and differential scanning calorimeter (DSC).

Rayleigh Scattering Photometry and POM. We employed time-resolved light scattering (LS) photometry to estimate the overall crystallization rate and its kinetics in the supercooled state of PP-MA and PPCNs in the quiescent state. The thin sample of about 40 μm thickness was quickly transferred from the melt state to the Linkam hot stage, placed in the light scattering apparatus, set at the predetermined

10.1021/ma010852z CCC: $22.00
Published on Web 02/16/2002

temperature, and immediately after attaining the crystallization temperature, T_c, a time-resolved LS measurement was carried out in the temperature range of 70−110 °C. It should be mentioned here that there was some time lag between putting the sample on hot stage and to switch on the computer to collect the data which is ∼10 s, sufficient for the equilibration of temperature. The one-dimensional photometer was equipped with a 38-channel photodiode (PDA: Hamamastu Photinics Co.) array which facilitated the angular dependence of scattered light intensity with a time slice of 1/30 s.[6] The scattering angle θ_{LS} was covered between 1.4° and 30°. The radiation of polarized He−Ne laser of 632.8 nm wavelength was used vertically to the sample, and the scattering profile was observed at an azimuthal angle of 45° under H_v (cross-polarized) alignment. We also used a conventional Polaroid camera (camera length = 156 mm) to record the scattering patterns on a photographic film with an exposure time of 1/60 s.[6] The photographs were taken after full solidification of the sample.

We also measured spherulite growth rate of PP-MA and PPCNs in the temperature range between 110 and 135 °C. For the measurement of linear growth rate the thin samples were crystallized on the Linkam hot stage mounted on a polarizing optical microscope (POM) (Nikon OPTI-PHOTO2-POL), and the diameter of the developed spherulite was measured with time using a video recording system (Linkam RTVMS, Linkam Scientific Instruments, Ltd.). After crystallization, the samples were observed using POM and fitted with a color-sensitive plate to determine the sign of birefringence, and then photographs were taken. The details of POM observation were described in our previous paper.[7]

WAXD. The X-ray diffraction experiments were performed using a MXlabo diffractometer (MAC Science Co.) with Cu Kα radiation and graphite monochromator (wavelength, $\lambda = 0.154$ nm). The generator was operated at 40 kV and 20 mA. The crystallized samples were placed inside an aluminum sample holder at room temperature and were scanned at diffraction angle 2θ from 2° to 10° at the scanning rate of 0.5°/min.

DSC. The crystallized samples were characterized by using a temperature-modulated differential scanning calorimeter, operated in the conventional DSC mode (TMDSC, TA2920, TA Instruments) at the heating rate of 5.0 °C/min, to determine the heat of fusion ΔH and melting temperature T_m of PP-MA and PPCNs. The DSC was calibrated with indium before use.

TEM. The dispersibility of the clay particle in the matrix was checked by using TEM (H-7100 Hitachi Co.) operated at an accelerating voltage of 100 kV without staining. A thin layer of around 70 nm thick from the crystallized sample was sectioned at −80.0 °C using a Reichert ultra-microtome equipped with a diamond knife.

Dynamic Mechanical Characterization. Dynamic mechanical measurements were performed on the samples of $35 \times 12 \times 0.5$ mm^3 size crystallized at 70.0 and 130.0 °C (two extreme temperatures where intercalation were measured) using dynamic temperature ramp tests, on a Rheometrics dynamic analyzer (RDAII) in tension−torsion mode in the temperature range between −50.0 and 140.0 °C at the heating rate of 2.0 °C/min, keeping the strain amplitude of 0.05%. The angular frequency ω for the experiments was 6.28 rad/s.

Results and Discussion

Spherulitic Texture. Figure 1 shows the typical LS patterns under H_v optical alignment for PP-MA and PPCNs, crystallized at 70.0 °C for 20 min. The PP-MA shows four-leaf-clover pattern when it is crystallized at low temperature ($T_c \leq 100$ °C), suggesting a high ordering of both tangential (crosshatch) and radial lamellae in the spherulites.[8] In the POM observation, the spherulites with positive birefringence appeared clearly.

In contrast, for PPCNs, a smeared four-leaf-clover pattern is observed compared to the crystallized PP-MA. With gradual increase of the organophilic clay loading, less and less ordered spherulites with increasing scattering patterns, such as rodlike scattering patterns, are observed which are also confirmed from the POM of PPCNs crystallized at low T_c (≤100 °C). The rodlike scattering pattern is ascribed to the parallel arrangement of radiating primary lamellae and the disordered arrangement of crosshatch lamellae.[5,8] Diffuse maltese cross patterns with very weak positive birefringence were observed in the PPCNs. The weak positive birefringence is attributed to the low density of the crosshatched lamellae. During crystallization, the formation of the crosshatch lamellae may be restricted due to the narrow space of the range between 30 and 60 nm, which is surrounded by the well-dispersed clay particles in the PPCN matrix, as discussed in our previous paper.[5]

At high T_c (≥110 °C), as the sizes of the spherulites are big enough and out of range for the LS experiment, we observed them directly using POM. Figure 2 shows the typical spherulitic texture of PP-MA and PPCNs at $T_c = 130.0$ °C for 12 h. Obviously, the spherulite size gradually decreases with increasing clay content, and the interspherulitic region becomes broader. These spherulites exhibited negative birefringence and can be classified into the Padden and Keith[9] type II spherulite category. For isotactic PP, Lotz and Whittman have elucidated the origin of the birefringence and textural pattern as being attributable to complex crosshatching mechanism.[10] The negative birefringence is attributed to the sufficiently low fraction of crosshatched lamellae compared to the radial lamellae. Figures 1 and 2 show that the dispersed clay particles act as a nucleating agent, which is evident from the increase in the number density of nuclei causing smaller spherulite formation.

Crystallization Kinetics. Figure 3 shows a typical example of the time variation of the diameter of the spherulite D for PP-MA and PPCNs at 135 °C. A linear growth of D is seen in a range of t scale for PP-MA, PPCN2, and PPCN7.5. The linear growth rate G ($= {}^1/_2(dD/dt)$), defined as the initial slope of the plots, slightly increases with increasing clay content. From the extrapolation of D vs t plots, we estimated the onset time t_0, which corresponds to the induction time of the crystallization. The t_0 of both PPCNs decreases with clay content compared to the PP-MA matrix without clay. As discussed above, the reduction of t_0 in the PPCNs is attributed to the nature of the clay as the nucleating agent.

Figure 4 shows the T_c dependence of G and t_0. Here it should be mentioned that the equilibrium melting temperatures (T_m^0) of the PPCNs and PP-MA are the same. The T_m^0's were measured by isothermal crystallization at various temperatures by carrying out a Hoffman−Weeks plot[11] as shown in Figure 5. Both PPCN7.5 and PP-MA show the same value of 158 °C and that would nullify the effect of supercooling ΔT ($\equiv T_m^0 - T_c$) on G and t_0. For both PPCNs and PP-MA, G decreases with increasing T_c in the temperature range of 110−135 °C. However, for PPCNs, G shows almost the same value compared to that of PP-MA without clay. Despite the increase in clay content, the dispersed clay particles have not much effect on the crystallization and no big acceleration of G in the crystallization of the PPCNs. In the changes in t_0 with T_c, the PPCNs show a remarkably short time especially at high T_c, suggesting that the dispersed clay particles have some contribution to enhance the nucleation as mentioned above. From Figure 2, the number of heterogeneous nuclei N can be estimated from a rough approximation. That is,

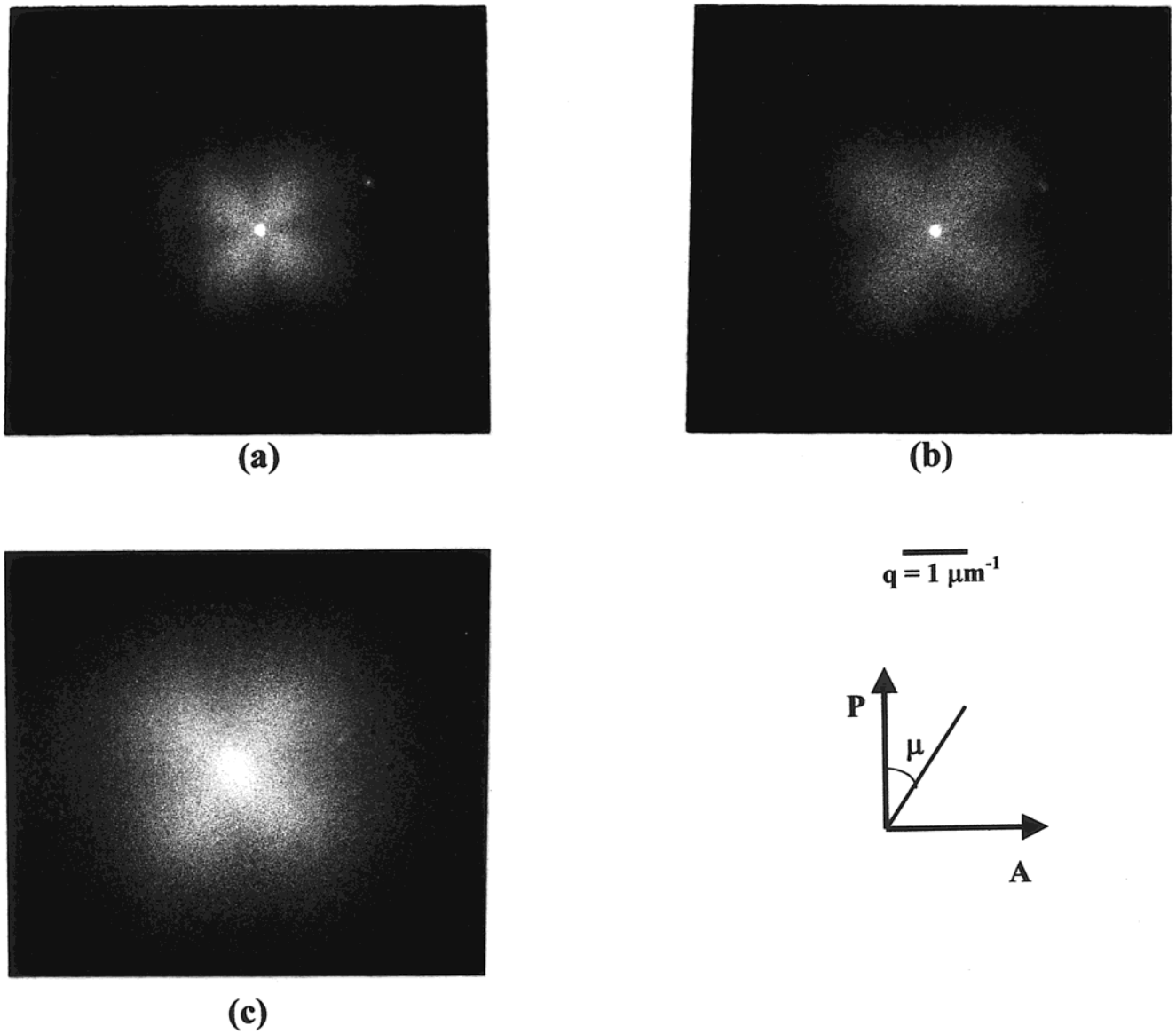

Figure 1. Typical H_v light scattering patterns after full solidification at $T_c = 70.0$ °C for (a) PP-MA, (b) PPCN2, and (c) PPCN7.5

all the spherulites are of identical size. The primary nucleation density of the spherulites, i.e., N was given by

$$N = (3/4\pi)(D_m/2)^{-3} \quad (1)$$

where D_m is the maximum diameter of the spherulite, i.e., the attainable diameter before impingement. The calculated value of N at 130 °C was 4×10^{-8} μm^{-3} for PP-MA, 50×10^{-8} μm^{-3} for PPCN2, and 200×10^{-8} μm^{-3} for PPCN7.5. The time variation of the volume fraction of the spherulites increases in proportion to NG^3 ($\cong$ overall crystallization rate). This fact suggests that the overall crystallization rates of the PPCNs are about 1 or 2 orders of magnitude higher than that of matrix PP-MA without clay.

To discuss the crystallization kinetics at low T_c ($\leq$100 °C), we employed time-resolved LS photometry, which is a powerful tool for estimating the overall crystallization rate and its kinetics in supercooled crystalline polymer liquids.[6] For the kinetics of crystallization, we can employ the integrated scattering intensity; i.e., the invariant Q is defined as

$$Q = \int_0^\infty I(q) q^2 \, dq \quad (2)$$

where q (scattering vector) $= (4\pi/\lambda_{LS}) \sin(\theta_{LS}/2)$, λ_{LS} is the wavelength of light in the specimen, θ_{LS} is the scattering angle, and $I(q)$ is the intensity of the scattered light at q.[12]

In the H_v mode the invariant Q_δ can be described by the mean-square optical anisotropy $\langle \delta^2 \rangle$:

$$Q_\delta \propto \langle \delta^2 \rangle \propto \phi_s (\alpha_r - \alpha_t)^2 \quad (3)$$

where ϕ_s is the volume fraction of spherulites and α_r and α_t are the radial and tangential polarizabilities of spherulites, respectively. We constructed a plot of reduced invariant Q_δ/Q_δ^∞ vs time t with Q_δ^∞ being Q_δ at an infinitely long time of crystallization (up to full solidification of the melt).

Figure 6 shows the time variation of the invariant Q_δ/Q_δ^∞ taken for PPCNs and PP-MA at 70 °C. The overall crystallization rate was determined from the slope of Q_δ/Q_δ^∞ ($d(Q_\delta/Q_\delta^\infty)/dt$) in the crystallization region as indicated by the solid line in Figure 6, and we plotted

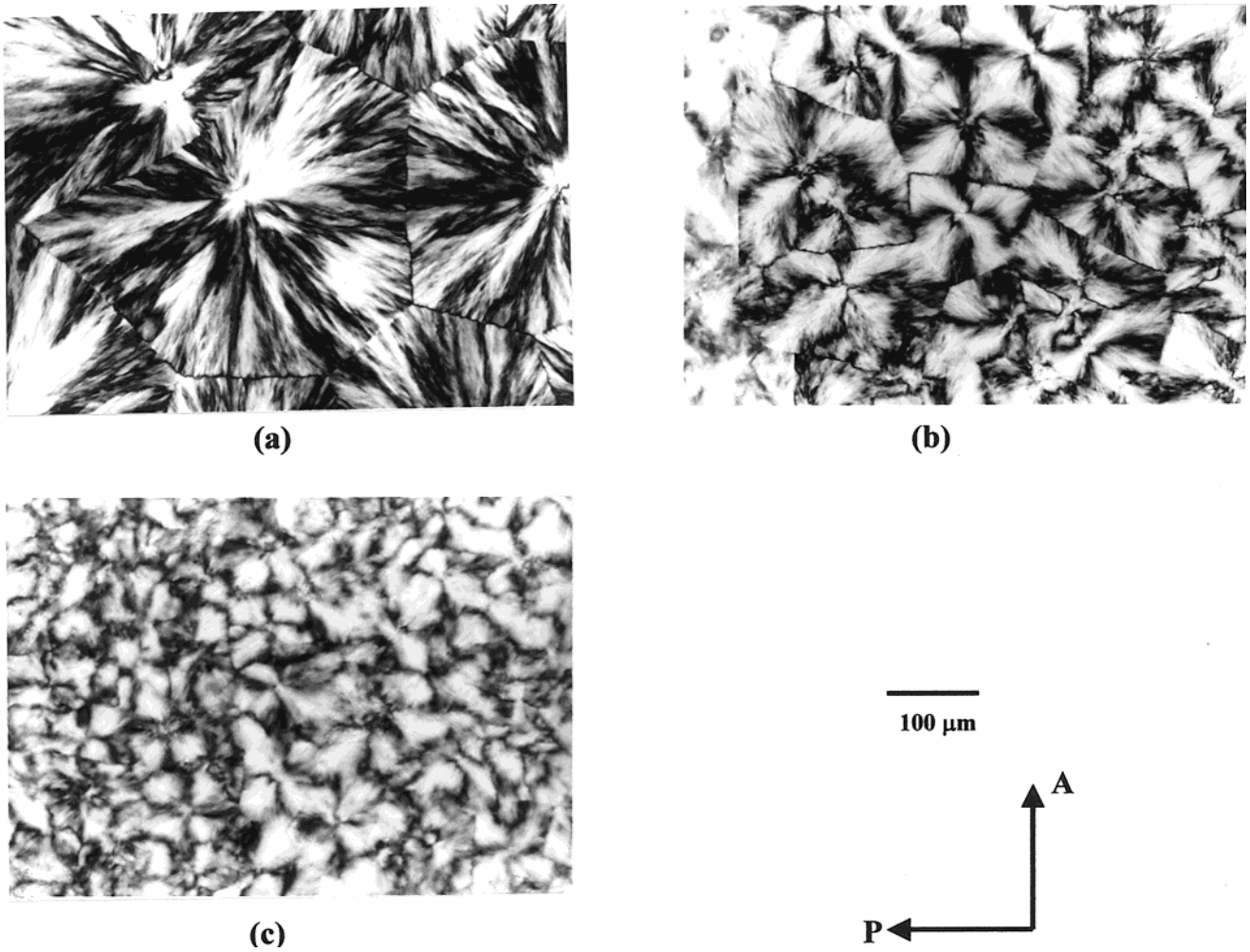

Figure 2. Optical micrographs of PP-MA and PPCNs crystallized after full solidification at 130.0 °C: (a) PP-MA, (b) PPCN2, and (c) PPCN7.5

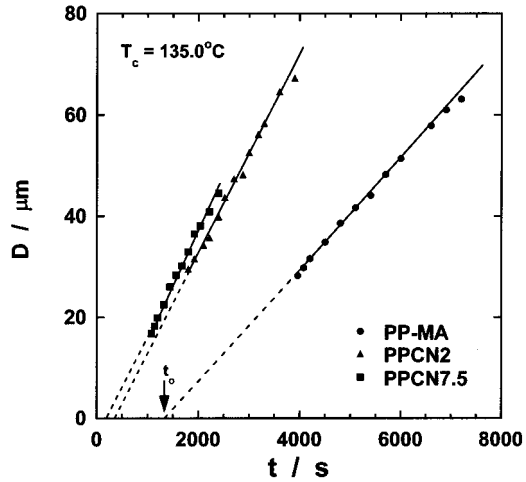

Figure 3. Spherulitic diameter as a function of crystallization time at $T_c = 135.0$ °C. The arrow indicates the induction time of crystallization for PP-MA.

it in Figure 7 against T_c. At low T_c ($\leq$100 °C) the overall crystallization rate of PPCNs exhibits a higher value than that of the matrix PP-MA and increases with the clay content. However, there is no big difference between PPCNs and matrix PP-MA as expected from results of the crystallization at high T_c ($\geq$110 °C). The nucleation of the matrix PP-MA without clay is enhanced due presumably to the increase of ΔT as in any conventional crystalline polymer,[13,14] while the PPCNs exhibit a

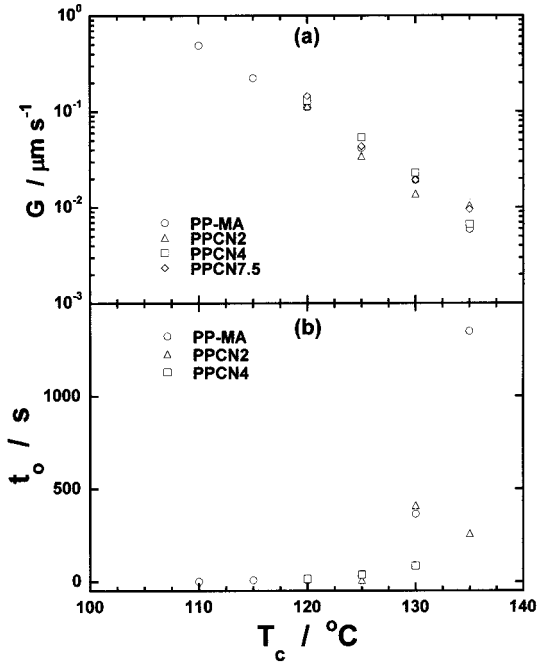

Figure 4. (a) Linear growth rate as a function of T_c and (b) induction time as a function of T_c. The induction time was calculated from the onset time as shown in Figure 3.

heterogeneous nucleation kinetics with weak ΔT dependence originating from the well-dispersed clay par-

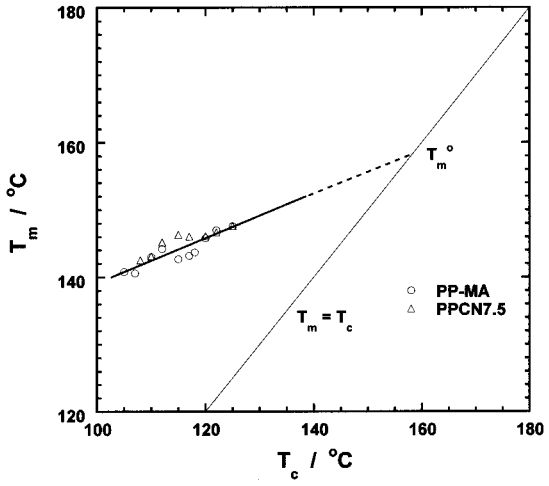

Figure 5. T_m vs T_c (Hoffman−Weeks) plots of PP-MA and PPCN7.5.

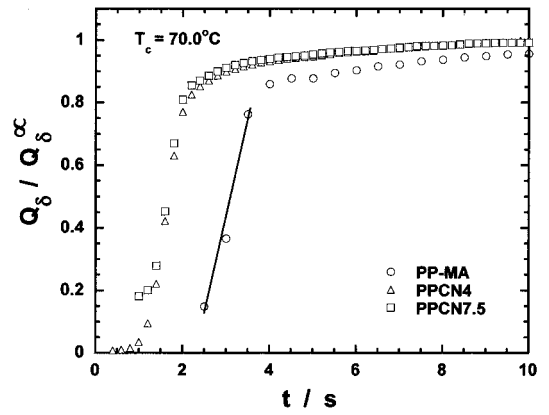

Figure 6. Time variation of reduced invariant Q_δ/Q_δ^∞ during isothermal crystallization at quiescent state at $T_c = 70.0$ °C. The solid line represents the slope (overall crystallization rate).

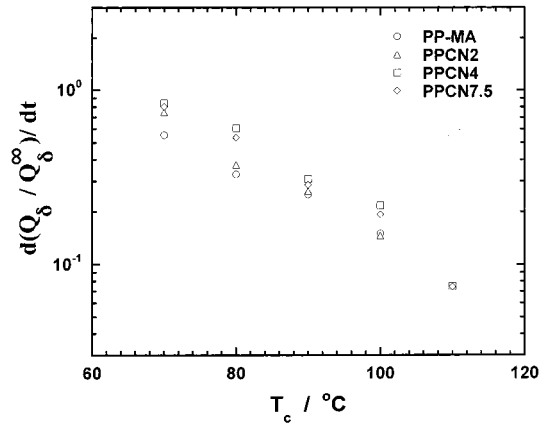

Figure 7. T_c dependence of the overall crystallization rate of PP-MA and PPCNs.

ticles in the matrix. Here, we should mention that there is some difference in the absolute value of linear growth rate (Figure 4) and overall crystallization rate (Figure 7), if we extrapolate the T_c region. The reason behind this is the measurement techniques. Two-dimensional growth is measured by POM while three-dimensional growth including the nucleation phenomena is observed in LS.

Segregation of Dispersed Clay Particles. To check the segregation of the dispersed clay particles

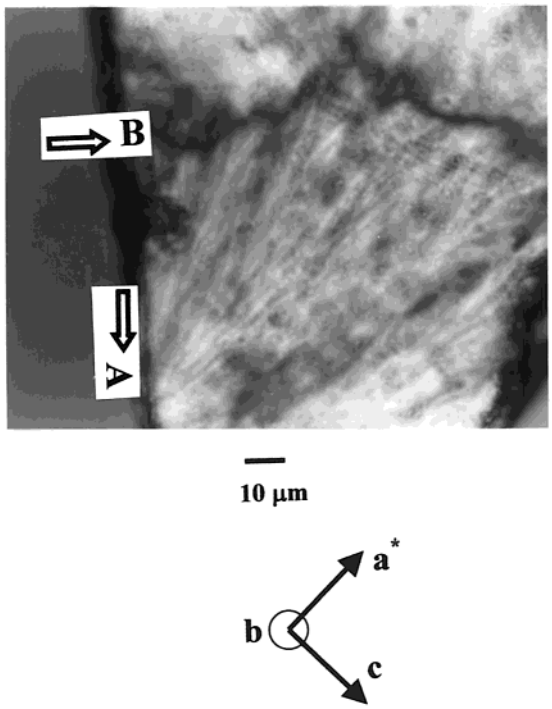

Figure 8. Optical micrograph of PPCN4 crystallized at 140.0 °C after full solidification. The arrows represent (A) inside spherulite and (B) interspherulitic position, respectively, where *a**, *b*, and *c* are the crystallographic axes.

between inside spherulite and interspherulitic regions, we carried out TEM in the spherulite of PPCN4, crystallized at 140 °C for 5 days. The spherulite under investigation is really three-dimensional in nature owing to its unusually large thickness of about 200 μm. The positions are shown by the arrows A (inside spherulite) and B (interspherulitic region) in Figure 8. Figure 9 shows TEM images of the different portions of the spherulite corresponding to Figure. 8. For each portion, we observed fine and uniform dispersion of the clay particles with lateral dimensions ranging of 100−200 nm in the matrix PP-MA where most of the clay particles (edges of the silicate layer) exhibit perpendicular alignment to the sample surface. Obviously, in the interspherulitic region (Figure 9b), a higher density of dispersed clay particles is observed compared to the density inside the spherulite (Figure 9a). *a** is the radial direction of spherulite, which is also the reciprocal lattice direction, *c* is the chain axis direction, and *b* is the other crystallographic axis. The correlation lengths of silicate layers (ξ_{layer}), calculated from average distance between two neighbor silicate layers, are 52 and 39 nm for inside spherulite and interspherulitic regions, respectively. On the contrary, PPCN4, crystallized at low T_c (<100 °C), exhibits uniform distribution of its silicate layers ($\xi_{layer} = 49$ nm).[5] The excess clay particles in the interspherulitic region are presumably the result of the segregation of the clay particles from the crystal growth front due to the exclusion. This segregation phenomenon may be suppressed at low T_c where the crystallization rate is high enough to solidify the system quickly. As discussed in the section of spherulitic texture, the broadness of the interspherulitic region may suggest a higher density of the dispersed clay particles.

Intercalation during Crystallization. At high T_c (≥110 °C), where the crystallization rate is low enough to solidify the system, the intercalation should be anticipated in the melt state during crystallization.[1] The

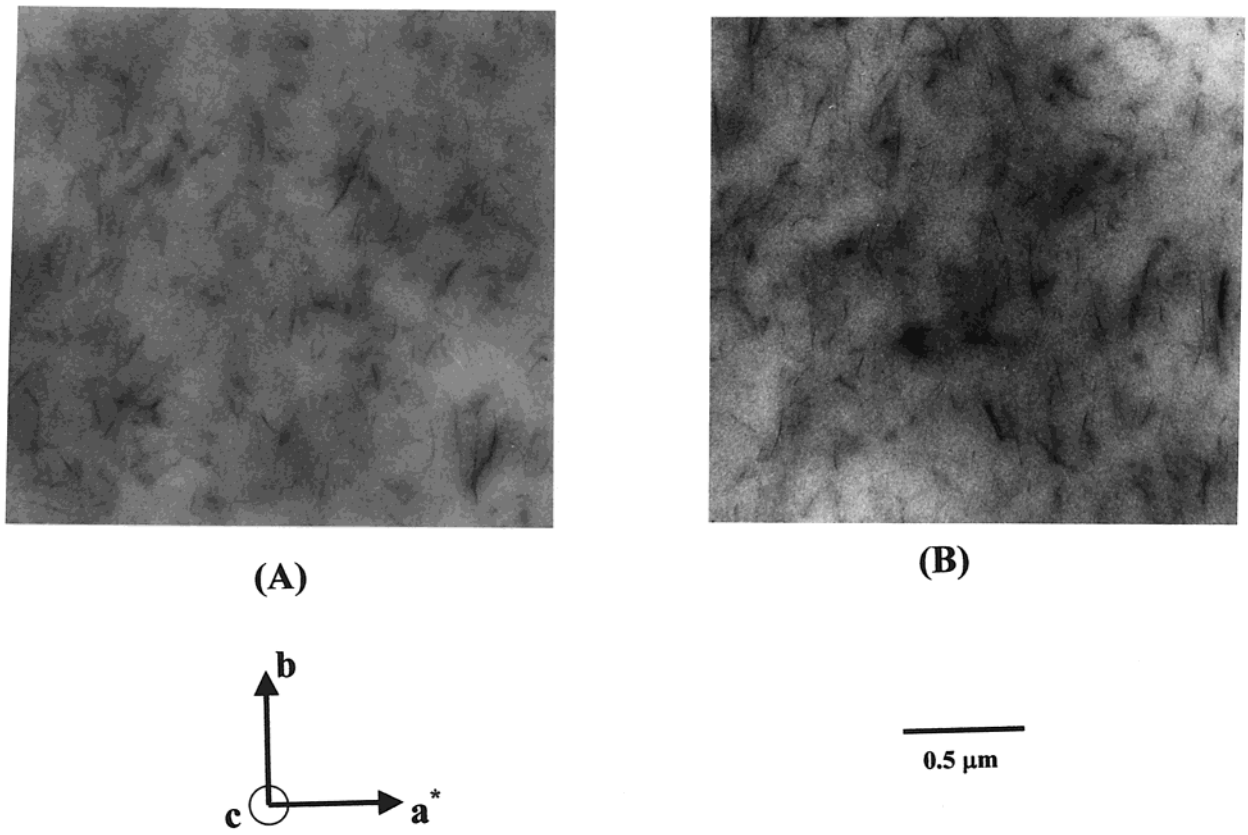

Figure 9. Typical transmission electron micrographs of PPCN4 crystallized 140.0 °C taken in two different positions as shown in Figure 8: (A) inside spherulite and (B) interspherulitic position.

driving force of the intercalation originates from strong hydrophilic interaction between the MA group and the polar clay surfaces.[4,5] WAXD patterns of PPCNs in the range of $2\theta = 2°-10°$ for crystallization at different T_c are shown in Figure 10. The WAXD patterns were taken after full solidification of the sample. The mean interlayer spacing of the (001) plane ($d_{(001)}$) for the organophilic clay solid obtained by WAXD measurements is 2.31 nm ($2\theta = 3.82°$) as indicated by the broken line in the figure. For each PPCN, we see a small remnant shoulder for PPCN2 and PPCN4 and a small peak for PPCN7.5, corresponding to the (001) plane of silicate layers due to the intercalation of the PP-MA chains in the silicate galleries. Clearly, with increasing T_c, the small peak and shoulder shift toward the smaller angle region in the PPCNs, suggesting that the extent of intercalation takes place with crystallization.

Figure 11 shows $d_{(001)}$ of the clay gallery quantitatively, as a function of T_c, obtained from their respective Bragg reflections. Here, in the case of PPCN2, the peak is not prominent (in fact, this system is partially exfoliated as confirmed from its TEM images in our previous paper[5]), and hence we did not perform the calculation of $d_{(001)}$ of this system. The dotted line shows the effect of annealing on the $d_{(001)}$ value of organoclay. The $d_{(001)}$ increases with T_c for both PPCN4 and PPCN7.5 systems, and PPCN4 exhibits always significantly a higher value than that of PPCN7.5. These imply that intercalation proceeds at T_c and increases with decreasing clay content. Further decrease of clay content from 4 to 2 wt % in PPCN2 leads to a partially exfoliated system as discussed above. That is, the PPCN with low clay content crystallized at high T_c (≥110.0 °C) exhibits a higher amount of intercalation than that with high clay content crystallized at any T_c.

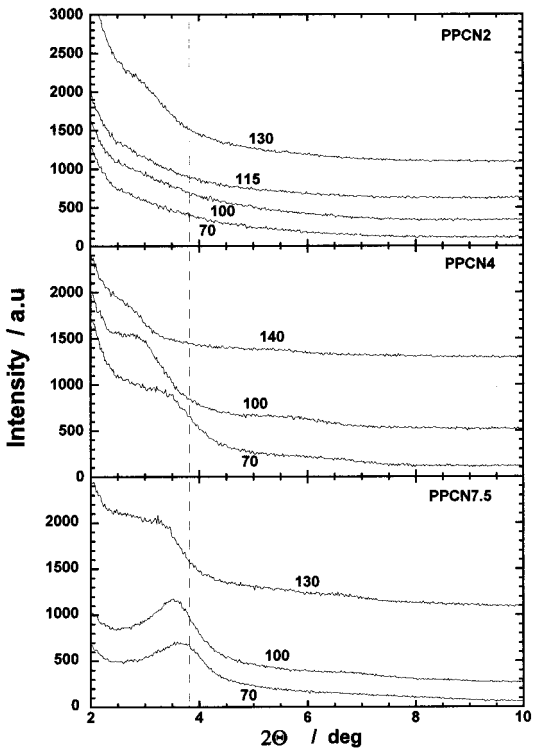

Figure 10. Typical WAXD patterns of PP-MA and PPCNs samples crystallized at different T_c as shown in the figure. The broken line indicates the peak position of organophilic clay solid. The data in the *y*-axis direction was shifted to avoid data overlap.

At high T_c (≥110 °C) (low crystallization rate), the melt state exists for quite a long time, and PP-MA chains have enough time to intercalate before crystal-

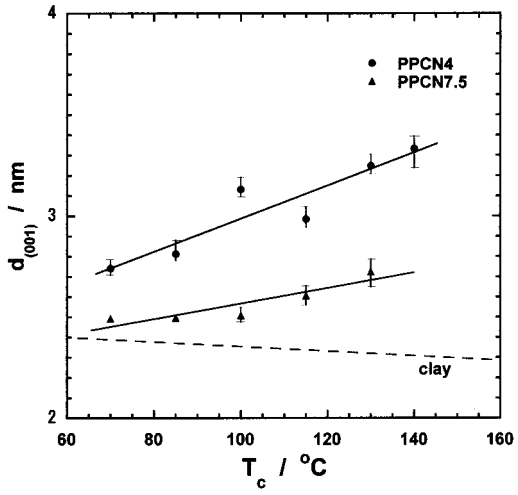

Figure 11. T_c dependence of the interlayer spacing of PPCN4 and PPCN7.5. The broken line shows the annealing effect on organoclay.

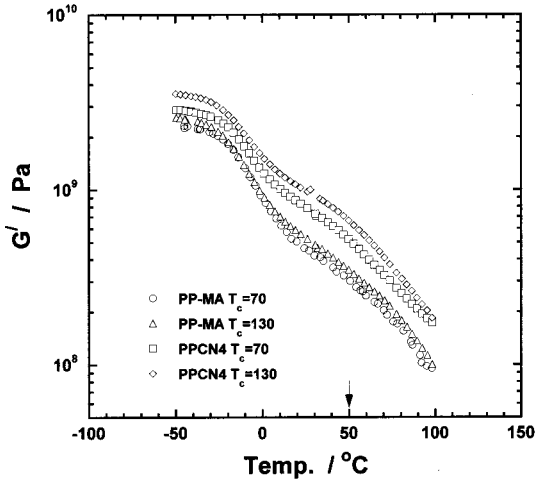

Figure 12. G' of PP-MA and PPCN4 crystallized at 70 and 130.0 °C as a function of temperature.

Scheme 1

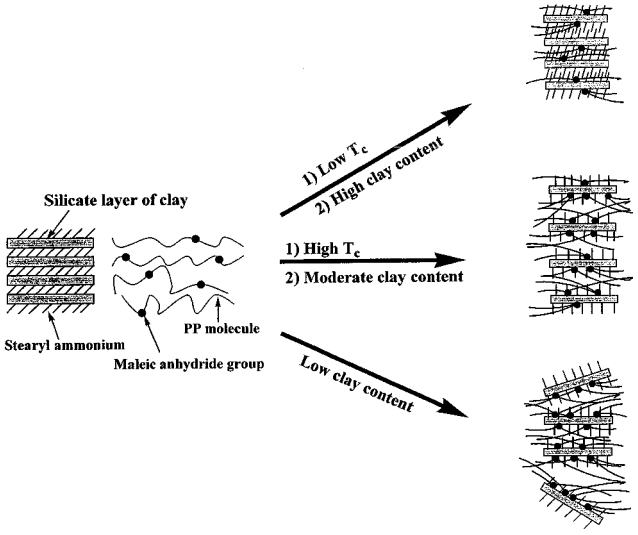

lization can occur in the bulk. Then, the enhanced intercalation is produced. Similar behavior is also manifested in the inside and interspherulitic region as revealed from TEM bright field images. In the interspherulitic region the intercalation is higher (width of silicate layer = 3.4 nm) than that of inside spherulite (width = 3.0 nm), presumably due to the higher melt state duration in the interspherulitic region. On the other hand, at low T_c (≤100 °C), the insufficient time makes less intercalation due to the high crystallization rate and lower chain diffusion compared to high T_c. The extent of intercalation is strongly dependent on the time of the molten state. In other words, the intercalated PPCNs are not equilibrated. By decreasing the clay content in the nanocomposites, the virtual gallery space in the silicate layers decrease, and consequently, the PP-MA molecules would try to accommodate, through interaction, in the minimum space causing higher intercalated species. For sufficiently low clay content, a system, like PPCN2, having less gallery space, is partially exfoliated due to high number density of tethering junction. Now it is necessary to understand the mechanism of intercalation.

Mechanism of Intercalation. There are two possible ways of ordering of polymer chains inside the silicate gallery by either (1) polymer molecules escape from gallery and crystallize outside (*diffuse out*) or (2) molecules may penetrate into the silicate gallery when they are in the molten state (*diffuse in*). When PPCN4 is directly crystallized from the melt at 70.0 °C for two different times of 30 min and 17 h, the interlayer spacing is the same (2.75 nm). If PPCN4 melt is annealed at 150.0 °C, just above T_m (=145.0 °C) for a sufficiently long time and then subsequently crystallized at 70.0 °C for 30 min, the interlayer spacing increases to 2.96 nm. Furthermore, when PPCN4 is crystallized from the melt at 30 °C, where crystallization rate is slow enough, the interlayer spacing becomes 3.08 nm. All these experiments indicate that the extent of intercalation is strongly dependent on the time of the molten state and ordering of polymer chains occurs through a *diffuse-in* mechanism. In other words, a slower crystallization rate makes a more intercalated species as molten polymer molecules have sufficient time to diffuse into the silicate gallery. On the basis of the WAXD and TEM micrographs, the nature of intercalation has been represented in Scheme 1. Thus, by suitably crystallizing the PPCNs, we can control the fine structure (*confined orientation*)[15] of the nanocomposites.

As discussed in our previous papers,[5] here, the effect of the degree of intercalation of PP-MA chains on the enhancement of the mechanical properties should be discussed.

Dynamic Behavior. According to Khare et al.'s[16] prediction, the confinement of polymer chains increases the viscosity and mechanical properties of the system significantly. We may expect some difference in mechanical properties with the change of the degree of intercalation in the PPCNs vis-à-vis the clay content and T_c. Accordingly, we measured the temperature dependence of storage modulus G' of the PPCN4 and PP-MA crystallized at two extreme temperatures of 70 and 130 °C as shown in Figure 12. Here, it can be mentioned that for a particular experimental condition of strain amplitude and frequency one can get the absolute value of G' at a fixed temperature. We compared the G' of different systems at a particular temperature (at 50 °C), keeping the fixed strain amplitude of 0.05% and angular frequency, ω of 6.28 rad/s in the strain-controlled rheometer. A slight increase of G' is observed for PP-MA crystallized at 130 °C compared to the sample crystallized at 70 °C, while a significant

Table 1. Storage Modulus of PP-MA and PPCNs at T = 50.0 °C Crystallized at Different Temperatures

system	T_c/°C	$G' \times 10^{-8}$/Pa	% increase
PP-MA	70	2.92	9.9
	130	3.21	
PPCN2	70	4.79	
	130	4.50	
PPCN4	70	5.16	30.6
	130	6.74	
PPCN7.5	70	7.49	13.3
	130	8.49	

increase appears in the case of the PPCN4. The G' values obtained at 50 °C for PP-MA and different PPCNs crystallized at two extreme temperatures are summarized in Table 1. It is clear from the table that, for a particular T_c, G' increases with increasing clay content. The PP-MA crystallized at 130 °C exhibits a 9.9% increase in G' compared to the sample crystallized at 70.0 °C. The PPCN7.5 and PPCN 4 show 13.3 and 30.6% increases, respectively, under the same conditions. The effect of T_c on the G' is in the order PP-MA < PPCN7.5 < PPCN4. It may be recalled that the T_c dependence of $d_{(001)}$ showed the order of intercalation PPCN7.5 < PPCN4 in Figure 11. This implies that much higher efficiency of the intercalation for the reinforcement is attained in the PPCN4. For PPCN2, owing to the partial exfoliation, the degree of intercalation decreases, and hence the modulus decreases compared to the low T_c condition (=70 °C). Here, it should be mentioned that the crystallinity increases little bit with increasing T_c (from 70 to 130 °C) for both PP-MA (χ_c = 29.1−34.5%) and PPCN4 (χ_c = 32.1−38.2%) for the above respective T_c, and the extent of increase is almost the same (∼5.5%) for these two systems. χ_c (=$\Delta H/\Delta H°$) is the crystallinity, considering the $\Delta H°$ is equal to 165 J/g.[14] So, it is believed that not the crystallinity but the degree of intercalation does affect the storage modulus.

Furthermore, there is another factor that lies in the PPCNs structure, as modulus is supposed to be determined by the stiffness of intercrystalline regions, specifically interspherulitic regions. The segregation of the dispersed clay particles is favored at high T_c, and thus, the concentration of the clay in the interspherulitic region becomes high as shown in Figure 9. This exclusion behavior may not be allowed at low T_c where crystallization time is short enough. Higher amounts of clay particles in the interspherulitic region may lead to higher modulus of PPCNs crystallized at high T_c.

Conclusions

The clay particles act as a nucleating agent for the matrix PP-MA, but the linear growth rate or overall crystallization rate is not influenced much in the presence of clay. Crystallization is one of the effective processes to control the extent of intercalation of polymer chains into silicate galleries and hence the mechanical property of the PPCNs. WAXD reveals that the intergallery spacing increases with T_c for any amount of clay content in PPCNs, and at constant T_c the extent of intercalation increases with decreasing clay content. The order of the extent of intercalation is PPCN7 < PPCN4 < PPCN2, and in fact, PPCN2 is partially exfoliated as revealed from TEM images and the weak WAXD peak.[5] The microstructure of nanocomposites as investigated by using TEM showed that the clay particles are well-dispersed at low T_c, and segregation of silicate layers occurs at high T_c. With the increase of T_c, G' increases, and that enhancement is maximum (30%) for PPCN4 while for PPCN7.5 it is only 13%. So, the intercalation has a strong influence on the mechanical properties of nanocomposites. Thus, by controlling the intercalation through crystallizing at a suitable temperature, one can control the fine structure (*confined orientation*), morphology, and mechanical properties of crystalline polymer/clay nanocomposites.

Acknowledgment. The present work was partially supported by the Grant-in-Aid for Academic Frontier Center under the project "Future Data Storage Materials" granted by the Ministry of Education, Science, Sports and Culture (1999−2003).

References and Notes

(1) Vaia, R. A.; Ishii, H.; Giannelis, E. P. *Chem. Mater.* **1993**, *5*, 1694. Vaia, R. A.; Teukolsky, R. K.; Giannelis, E. P. *Chem. Mater.* **1994**, *6*, 1017. Vaia, R. A.; Jandt, K. D.; Kramer, E. J.; Giannelis, E. P. *Macromolecules* **1995**, *28*, 8180. Vaia, R. A.; Vasudevan, S.; Krawiec, W.; Scanlon, L. G.; Giannelis, E. P. *Adv. Mater.* **1995**, *7*, 154.
(2) Kawasumi, M.; Hasegawa, N.; Kato, M.; Ushiki, A.; Okada, A. *Macromolecules* **1997**, *30*, 6333. Kato, M.; Usuki, A.; Okada, A. *J. Appl. Polym. Sci.* **1997**, *66*, 1781. Hasegawa, N.; Kawasumi, M.; Kato, M.; Usuki, A.; Okada, A. *J. Appl. Polym. Sci.* **1998**, *67*, 87. Usuki, A.; Kato, M.; Okada, A.; Kurauchi, T. *J. Appl. Polym. Sci.* **1997**, *63*, 137.
(3) Hasegawa, N.; Okamoto, H.; Kato, M.; Usuki, A. *J. Appl. Polym. Sci.* **2000**, *78*, 1981.
(4) Hasegawa, N.; Okamoto, H.; Kato, M.; Tsukigase, A.; Usuki, A. *Macromol. Mater. Eng.* **2000**, *280/281*, 76.
(5) Maiti, P.; Nam, P. H.; Okamoto, M.; Kotaka, T.; Hasegawa, N.; Usuki, A. *Polym. Eng. Sci.*, in press. Nam, P. H.; Maiti, P.; Okamoto, M.; Kotaka, T.; Hasegawa, N.; Usuki, A. *Polymer* **2001**, *42*, 9633.
(6) Kubo, H.; Sato, H.; Okamoto, M.; Kotaka, T. *Polymer* **1998**, *39*, 501.
(7) Okamoto, M.; Kubo, H.; Kotaka, T. *Polymer* **1998**, *39*, 3135.
(8) Norton, B. R.; Keller, A. *Polymer* **1985**, *26*, 704.
(9) Padden, F. R., Jr.; Keith, H. D. *J. Appl. Phys.* **1959**, *17*, 473.
(10) Lotz, B.; Wittmann, J. C. *J. Polym. Sci., Polym. Phys. Ed.* **1986**, *24*, 1541.
(11) Martuscelli, E.; Silvestre, S.; Abate, G. *Polymer* **1982**, *23*, 229.
(12) Okamoto, M.; Inoue, T. *Polymer* **1995**, *36*, 2736.
(13) Okamoto, M.; Shinoda, Y.; Kinami, N.; Okuyama, T. *J. Appl. Polym. Sci.* **1995**, *57*, 1055.
(14) Moore, E. P., Jr. *Polypropylene Handbook*; Hanser/Gardner: Cincinnati, OH, 1996.
(15) The higher extent of *confined orientation* of polymer molecules in between silicate galleries (so-called intercalation) of PPCN4 compared to PPCN7.5 can also be proved from its higher heat of fusion. As the interlayer spacing is limited (2−3 nm), it is believed that crystallization is difficult, but one may expect the extra heat of fusion from that type of orientation inside the silicate gallery (as shown in Scheme 1) when they are subjected to heating from room temperature to T_m.
(16) Khare, R.; Pablo, J. J.de.; Yethiraj, A. *Macromolecules* **1996**, *29*, 7910.

MA010852Z